Full Length Article

Density functional theory study of lignin, carboxymethylcellulose and unsustainable binders with graphene for electrodes in lithium-ion batteries

Veerapandian Ponnuchamy [a,b,*], Esakkiammal Sudha Esakkimuthu [a]

[a] *InnoRenew CoE, Livade 6, Izola 6310, Slovenia*
[b] *University of Primorska, Andrej Marušič Institute, Titrov trg 4, Koper 6000, Slovenia*

ARTICLE INFO

ABSTRACT

Electrodes are the fundamental components in lithium-ion batteries to develop high-performance device systems. The fabrication process of electrodes involves a mixing of active materials, a nonconductive polymeric binder material, and an electrically conductive additive. Binders play a critical role during the electrochemical process, which tightly holds the active materials together within the electrode to provide a long-cycle life. The present study investigates the strength of the interaction for different binders such as vinylidene fluoride (VDF), pyrrole (PY), styrene-butadiene (SB), acrylonitrile (AN), tetrafluoroethylene (TFE), carboxymethylcellulose (CMC), and lignin monomers, coumarylalcohol (LCmA), coniferylalcohol (LCnA), and sinapylalcohol (LSiA), using density functional theory calculations. The result reveals that sustainable binders (CMC, LCmA, LiCnA, and LSiA) exhibit higher interaction energy than unsustainable binders (VDF, PY, SB, AN, and TFE). The highest interaction energy is obtained for the graphene-LiSiA system, followed by graphene-LCnA and graphene-LCmA. Comparing the orientation of the binders on the graphene surface, all binders make a face-to-face arrangement with graphene. This interaction is greatly enhanced for those binders that possess aromatic rings with functional groups (methoxy and hydroxyl). These results provide significant insights for the use of lignocellulosic biomass materials such as lignin and cellulose as binders in energy devices toward more sustainability.

1. Introduction

Binders are one of the most important materials used in lithium-ion batteries (LIB) and significantly influence the overall performance of the battery device towards a long life. The typical LIB electrode is composed of a mixture of active lithium metal oxide-based electrode material for cathode (and usual graphite for the anode), polymeric binder material, and electrically conductive material on the electrical current collector. Therefore, the stability of electrode materials is indispensable to ensure device functions. Currently, there has been a tremendous amount of research attempting to develop a high current capacity for LIB electrodes. During the charging and discharging process, significant changes have occurred at the electrodes and the most important is volume change, which potentially increases the stress inside the material and eventually undergoes device deterioration. One of the solutions is to use polymeric binder materials to overcome this particular issue since binder materials play a vital role in the fabrication of electrodes. The authors have demonstrated that the optimization of binder material type and amount is fundamental to improve the energy density, stability, and

safety [1] and also provide an intrinsic adhesive property that enables resistance of volume changes during cycling performance. These binders are usually made of one or more polymeric components and should possess electrochemical stability and adequate mechanical properties.

Poly(vinylidene fluoride) (PVDF) polymer is the traditional binder material and widely used for the fabrication of both cathode and anode due to its high electrochemical stability, mechanical support, and high adhesive property that integrates electrodes and conductive materials [2–4]. However, the main disadvantage of PVDF is that it is insoluble in water and requires an organic solvent, N-Methyl-2-pyrolidine (NMP), to process it into electrode slurry [5]. NMP is expensive and toxic and, therefore, the manufacturing process should be performed in a controlled way so that the solvent can be collected and reused without affecting the environment. As a consequence, the production cost for the entire process is significantly high in the industry [1]. Furthermore, PVDF exhibits insufficient bonding, low flexibility, and formation of stable LiF after reacting with lithium metal, which leads to capacity fading and short cycle-life [6–9]. Recently, much research has been devoted to seeking alternative binders that can be soluble in water to
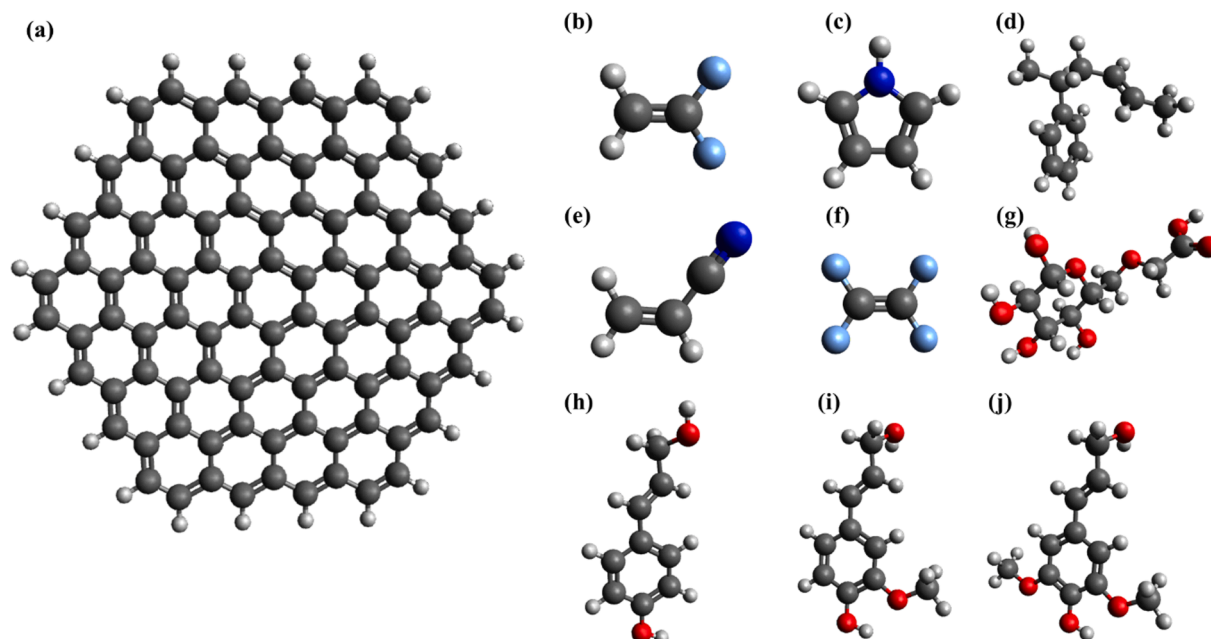

Fig. 1. Optimized isolated geometries of (a) graphene sheet ($C_{96}H_{24}$), (b) vinylidene fluoride (VDF), (c) pyrrole (PY), (d) styrene butadiene (SB), (e) acrylonitrile (AN), (f) tetrafluoroethylene (TFE), (g) carboxyl methyl cellulose (CMC) and lignin monomers, (h) coumaryl alcohol (LCmA), (i) coniferyl alcohol (LCnA), and (j) sinapyl alcohol (LSiA).

enhance the sustainability of LIBs without compromising electrochemical performance. The most commonly used alternative binders are carboxymethyl cellulose (CMC), styrene-butadiene (SB) rubber, pyrrole (Py), tetrafluoroethylene (TFE), and acrylonitrile (AN) [10–19]. Similarly, the second largest abundant biomass polymer, lignin, draws more attention for use in making anode electrodes and also as binder materials for LIBs due to its aromatic polymeric structure and high mechanical strength [20,21]. Lignin macromolecule is made up of three predominant monomer units, coniferyl alcohol, coumaryl alcohol, and sinapyl alcohol, through a random radical polymerization process [22]. The composition of the monomer units can depend on the type and origin of the plants[23]. Lignin is mainly produced as a by-product during pulping process in paper industry and mostly burnt for energy [24]. Therefore, the investigation of lignin has been growing in recent decades to valorize for various types of applications including fuels and chemicals [25,26], activated carbon for electrodes in supercapacitors[27–30] and batteries[31,32] and also binders for electrodes [21,33].

Apart from binders, the authors have attempted to study different types of graphite-based materials such as synthetic and natural flakes, natural and synthetic graphite powders as anode materials in Li-ion batteries[34–36]. Comparing synthetic and natural flakes anodes, both exhibit similar properties like irreversible capacity in ethylenecarbonate and alkyl carbonate electrolytes but these materials fail in propylenecarbonate electrolyte solutions[34]. On the other hand, natural graphite powders demonstrated good reversible capacities and negligible irreversible capacity losses due to low surface area in the rounded edges and absence of exfoliation than synthetic graphite powders [35].

Atomic structure calculations provide deep insights to understand the fundamental physical and chemical interactions between the materials such as graphene and binders. Several authors have performed numerous materials on the graphene surface to elucidate the strength of the interactions. Adeayo et al. studied the interaction strength between water and benzene to water on graphene by employing different GGA functionals and compared with random phase approximation (RPA) and CCSD(T) calculations [37]. The results showed the interaction energies differ up to ~ 1 kcal/mol and ~ 0.4 kcal/mol for CCSD(T) in the case of lower polycyclic aromatic hydrocarbons (PAHs: C_6, C_{24} and C_{54} carbons), and a similar trend was observed for larger PAHs up to C_{216} with

applied functionals. The range-separated *meta*-GGA ωB97M-V functional exhibits a quantitative agreement with RPA and CCSD(T). The binding interaction of carboxylic acids with PAHs (C_{24}, C_{54} and C_{98}) was studied and the results showed that the linear parallel configuration on the PAHs is preferable to the calculated binding enthalpy and Gibbs free energy calculations [38]. Similarly, various studies have investigated the interaction orientation of different molecules with PAHs to calculate their strength [39–42], but to the best of our knowledge, no studies have been focused to demonstrate the interaction of different organic binders and specifically lignin with graphene towards lithium-ion batteries.

In this work, graphene is considered as a model for graphite basal planes and we calculate the interaction strength between graphene and the monomer of different organic binders such as vinylidene fluoride, pyrrole, styrene-butadiene, acrylonitrile, tetrafluoroethylene, carboxymethylcellulose, and lignin monomers by employing DFT calculations. In particular, three monomers (coniferyl alcohol, coumaryl alcohol, and sinapyl alcohol) were considered for lignin macromolecule and understand their mechanism of interaction with graphene. The binding energy of all binders with a graphene sheet, considering possible orientations on the surface, was calculated and compared. The size of the graphene sheet was studied with a specific configuration of the binder (sinapyl alcohol) to evaluate the size effect that influence in the calculated interaction energy.

2. Computational details

The present study considers typical graphene, which consists of 37 benzene rings with chemical formula $C_{96}H_{24}$, and hydrogen atoms that were used at the edge of the graphene for termination. Similar composition of graphene was employed by different authors for various studies to calculate interactions[43]. Density functional theory (DFT) calculations were employed to investigate all electrotonic structure calculations using GAMESS-US package[44]. The initial geometry of graphene and all binder was optimized with ωB97X-D/6–31 g(d) level of theory. The single point energy calculations for graphene-binders were performed further with same functional (ωB97X-D) at higher level basis set 6–311 g (d,p) in order to calculate the interaction energy for the systems and the similar method was employed for other systems[45,46]. The ωB97X-D
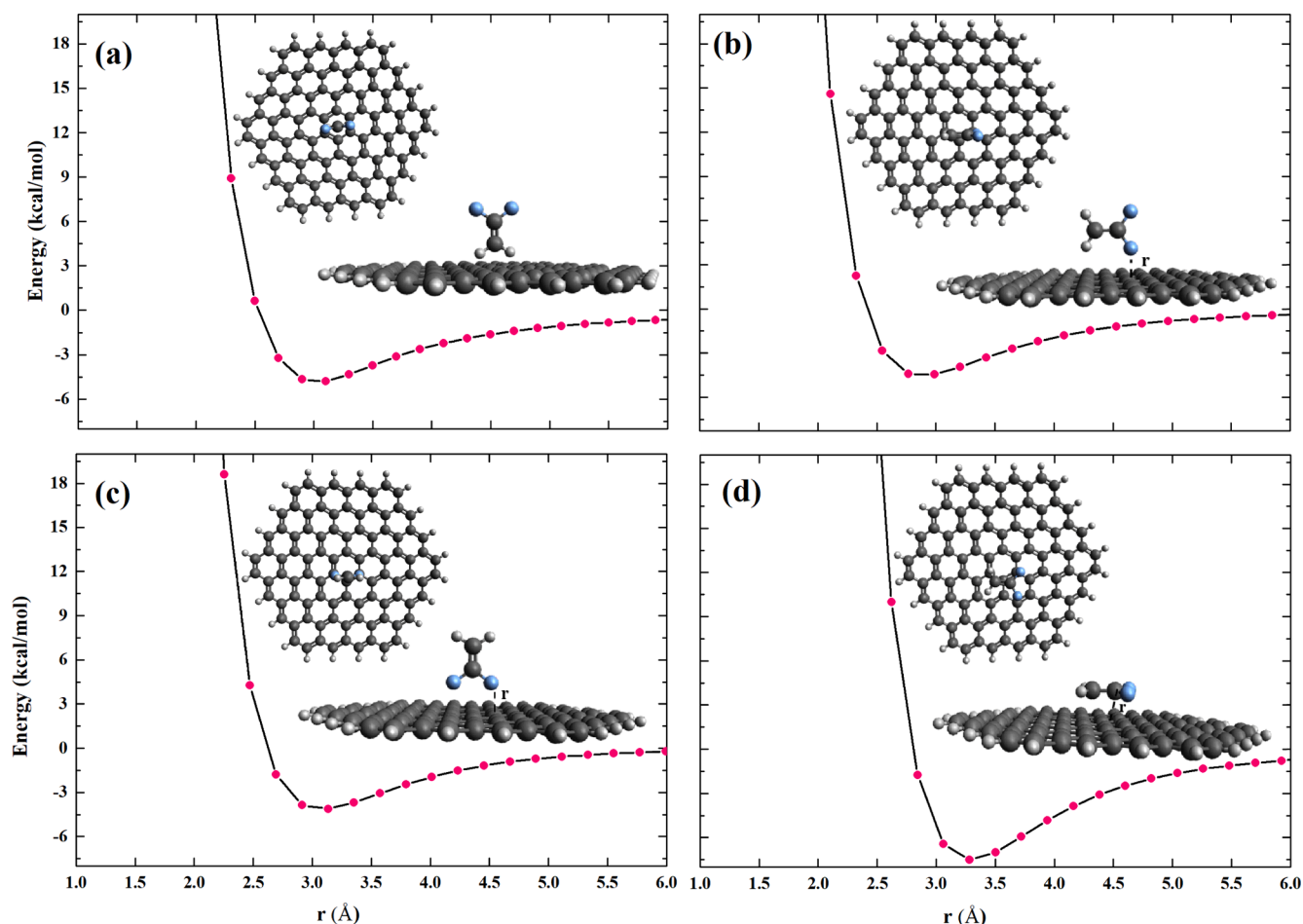
Fig. 2. Interaction energy curves with corresponding structural configuration of graphene-vinylidene fluoride systems: (a) graphene-vinylidene fluoride-perpendicular-hydrogens-down-on-bridge (GR-VDF-Per-H$_{down}$-On$_{Bridge}$), (b) graphene-vinylidene fluoride-perpendicular-hydrogen-fluorine-down-on-carbon (GR-VDF-Per-HF$_{down}$-OnC), (c) graphene-vinylidene fluoride-perpendicular-fluorines-down-on-carbon (GR-VDF-Per-F$_{down}$-OnC), and (d) graphene-vinylidene fluoride-face-face-fluorines-on-bridge (GR-VDF-FF-On$_{Bridge}$).

Table 1
Name of the configurations, interaction energies (in kcal/mol), and distances between graphene and binders (VDF, PY, SB, ACN, TFE) (in Å).

Configurations	Interaction Energy (kcal/mol)	Distance (Å)
Graphene-VDF		
GR-VDF-Per-H$_{down}$-On$_{Bridge}$	−4.79	3.100
GR-VDF-Per-HF$_{down}$-OnC	−4.46	2.986
GR-VDF-Per-F$_{down}$-OnC	−4.12	3.134
GR-VDF-FF-On$_{Bridge}$	−7.52	3.282
Graphene-PY		
GR-PY-Per-N$_{down}$-OnC	−6.65	2.344
GR-PY-FF-N-On$_{Bridge}$	−12.18	3.340
GR-PY-FF-N$_{ring-centre}$	−12.20	3.908
GR-PY-Per-C$_{down-centre}$	−4.62	2.953
Graphene-SB		
GR-SB-Per-PhAl$_{side-down}$	−15.79	2.837
GR-SB-Per-Al-F	−13.29	2.617
GR-SB-Per-Ph-F	−15.92	2.593
GR-SB-Per-Al-C$_{down}$	−6.17	2.908
Graphene-ACN		
GR-ACN-Per-N$_{down}$-C	−2.65	3.083
GR-ACN-Per-M$_{down}$	−5.31	2.658
GR-ACN-Per-A$_{down}$	−6.55	2.579
GR-ACN-FF-N-onC	−9.28	3.236
Graphene-TFE		
GR-TFE-Per-1C2F$_{down}$- On$_{Bridge}$	−4.30	2.917
GR-TFE-Per-2C2F$_{down}$- On$_{Bridge}$	−4.80	3.137
GR-TFE-FF- On$_{Bridge}$	−10.07	3.166
GR-TFE-FF-Bet-Ring$_{centre}$	−9.33	3.352

functional is a long-range hybrid DFT functional with damped atom–atom dispersion corrections and accounts for high consistent description for intermolecular interaction between molecules such as non-covalent interactions, thermochemistry, and kinetics[47]. This functional was successfully used for various systems like dimer interactions [48–50] and lignin-solvent interactions[45,46]. Furthermore, the authors have found that ωB97X-D/6–31 g(d) level of theory showed improved binding energy values among other levels employed for the calculation between polyaromatic hydrocarbon molecules, and their calculated results were in good agreement with experimental values [51]. Want et al. performed benchmark calculations to evaluate the performance of the different functionals in describing the adsorption of aromatic molecules on graphene and found that ωB97X-D, B-LYP-D3 and B97-D provide the best results compared to other functionals such as M05-2X, M06-2X and M11-L[52]. Similarly, the same ωB97X-D functional was employed for the recent work to study the isotopic effects on adsorption of benzene on the C54 carbon-based graphene sheet and found acceptable results [53].

The interaction energy of the examined systems was calculated based on the following expression as the energy difference between the combined graphene-binders system and corresponding isolated molecules,

$$\Delta E = 627.51 \times (E_{GB} - E_G - E_B), kcal\, mol^{-1} \qquad (1)$$

where E$_{GB}$ represents the graphene-binder system and E$_G$ and E$_B$ are the energies of isolated geometries of graphene and considered binder molecules, respectively.
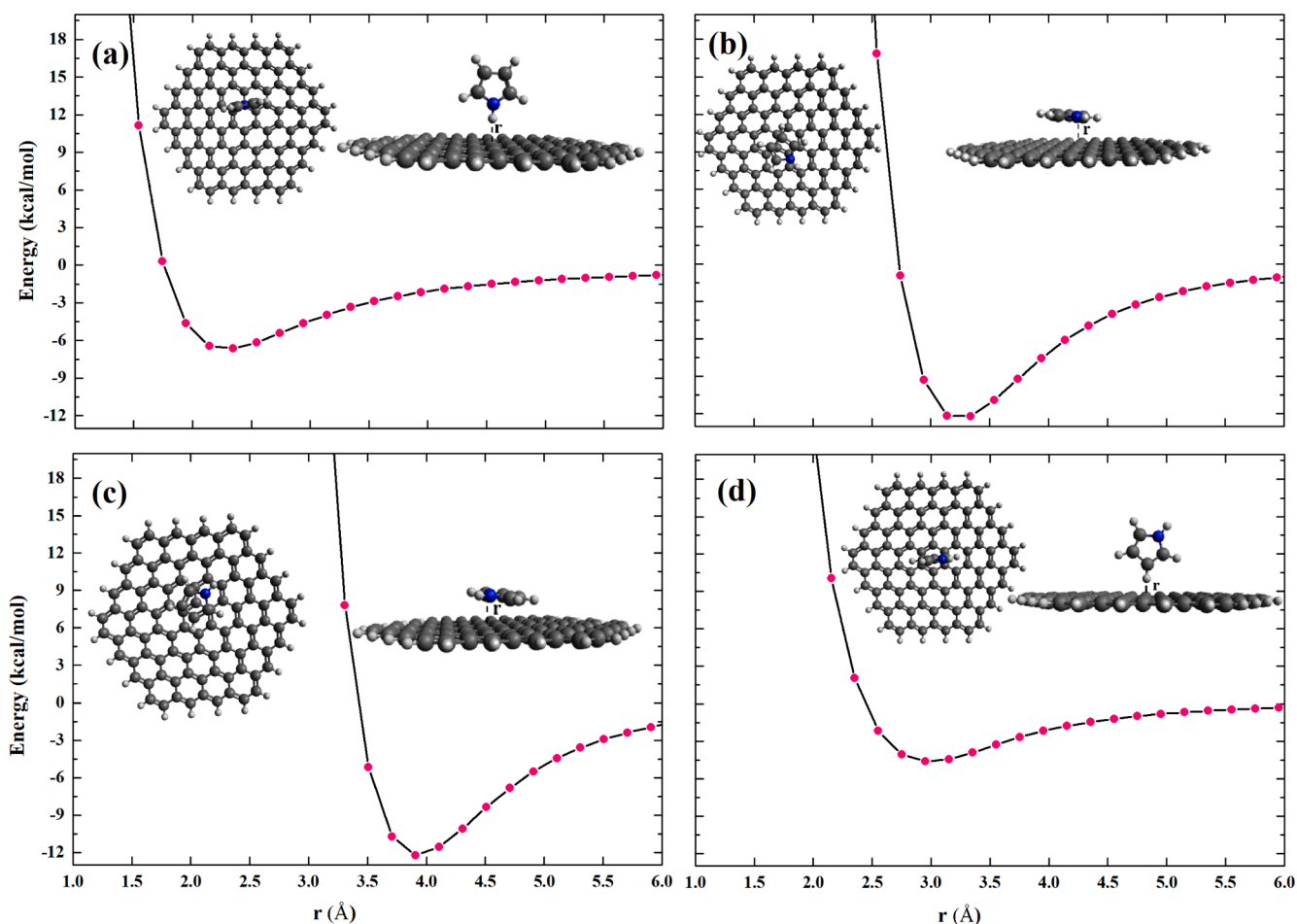
Fig. 3. Interaction energy curves with corresponding structural configuration of graphene-pyrrole systems: (a) graphene-pyrrole-perpendicular-Nitrogen-down-on-carbon (GR-PY-Per-N_{down}-OnC), (b) graphene-pyrrole-face-face-Nitrogen-on-bridge (GR-PY-FF-N-On$_{Bridge}$), (c) graphene-pyrrole-face-face-Nitrogen-ring-center (GR-PY-FF-$N_{ring-centre}$), and (d) graphene-pyrrole- perpendicular-carbon-down-centre (GR-PY-Per-$C_{down-centre}$).

3. Results

The isolated optimized geometries of the $C_{96}H_{24}$ graphene sheet and different examined binders in the gas phase at ωB97X-D/6–31 g(d) level are shown in Fig. 1.

Polyvinylidene fluoride (PVDF) is the main binder material used in various devices for electrode fabrication, and corresponding vinylidene fluoride (VDF) monomer was considered for the present study with graphene to illustrate the possible interactions. In this regard, there are eight different configurations that have been considered: (a) graphene-vinylidene fluoride-perpendicular-hydrogens-down-on-bridge (GR-VDF-Per-H_{down}-On$_{Bridge}$), (b) graphene-vinylidene fluoride-perpendicular-hydrogen-fluorine-down-on-carbon (GR-VDF-Per-HF_{down}-OnC), (c) graphene-vinylidene fluoride-perpendicular-fluorines-down-on-carbon (GR-VDF-Per-F_{down}-OnC), (d) graphene-vinylidene fluoride-face-face-fluorines-on-bridge (GR-VDF-FF-On$_{Bridge}$), (e) graphene-vinylidene fluoride-perpendicular-hydrogen-fluorine-down-on-bridge (GR-VDF-Per-HF_{down}-On$_{Bridge}$), (f) graphene-vinylidene fluoride-perpendicular-fluorines-down-on-bridge (GR-VDF-Per-F_{down}-On$_{Bridge}$), (g) graphene-vinylidene fluoride-face-face-fluorines-OnC (GR-VDF-FF-OnC), and (h) graphene-vinylidene fluoride-perpendicular-fluorines-down-ring-center (GR-VDF-Per-F_{down}-Ring$_{center}$). Fig. 2 presents four configurations from (a) to (d) with associated interaction energy values in Table 1, and the remaining are shown in supporting information **Figure S1** with **Table S1**. It can be seen from Fig. 2 that the most possible interaction was found for the configuration formed by a face-to-face arrangement of VDF and graphene (GR-VDF-FF-On$_{Bridge}$) with the interaction energy

value of −7.52 kcal/mol. The second most possible interaction (-4.81 kcal/mol) was seen in the GR-VDF-Per-F_{down}-Ring$_{center}$ (**Figure S1**h) configuration where two fluorine atoms perpendicularly interacted with hexagonal rings' center of the graphene. Among the examined configurations, the least interaction energy was obtained for the GR-VDF-Per-F_{down}-OnC configuration in which the two fluorine atoms interacted directly through carbon atoms, leading to more attraction between C-F than face-to-face interaction. Moreover, comparing the different orientations of VDF on graphene, the perpendicular and sideway interactions exhibit similar interaction energy values with the range between −4.0 to −4.79 kcal/mol.

In the case of graphene-pyrrole interaction, eight different configurations were studied based on the orientation of pyrrole molecule on the graphene surface to find the most viable binding interactions. Among the investigated configurations, four important configurations were shown in Fig. 3, containing the highest interaction energy and the least interaction energy and other configurations, such as (e) and (h), are illustrated in the supporting information (**Figure S2**). In the GR-PY-Per-N_{down}-OnC case, presented in Fig. 3a, the nitrogen atom with a hydrogen of the pyrrole molecule interacted on the graphene carbon atom with the interaction energy about −6.65 kcal/mol. Moreover, similar to the GR-PY-Per-$N_{down-centre}$ configuration, the pyrrole ring was placed at the hexagonal ring of the graphene for GR-PY-Per-$N_{down-center}$ configuration (f), as shown in **Figure S2**f, and obtained a −6.71 kcal/mol interaction energy. The difference in interaction energy for these two configurations is relatively small (0.16 kcal/mol) which demonstrates that the interaction of hydrogen attached with nitrogen to graphene shows no
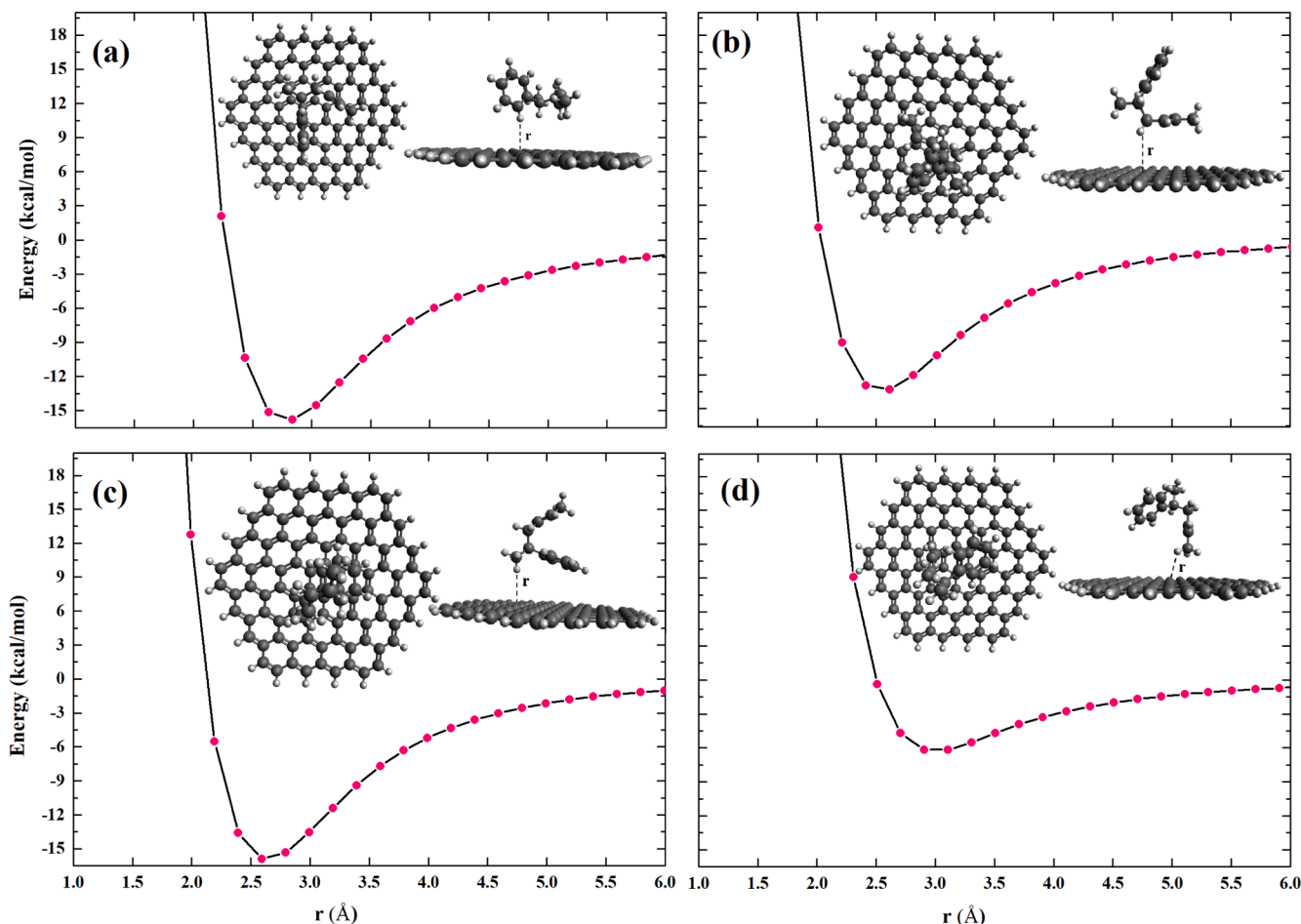
Fig. 4. Interaction energy curves with corresponding structural configuration of graphene-styrene butadiene systems: (a) graphene-styrene butadiene-perpendicular-phenyl-aliphatic-side-down (GR-SB-Per-PhAl$_{side-down}$), (b) graphene-styrene butadiene-perpendicular-aliphatic-face (GR-SB-Per-Al-F), (c) graphene-styrene butadiene-perpendicular-phenyl-face (GR-SB-Per-Ph-F), and (d) graphene-styrene butadiene-perpendicular-aliphatic-chain-down (GR-SB-Per-Al-C$_{down}$).

differences irrespective of the position. In the case of GR-PY-FF-N-On$_{Bridge}$ configuration, depicted in Fig. 3**b**, the nitrogen atom was placed between the carbon atoms in graphene, whereas, the nitrogen atom was at the center of hexagonal graphene for GR-PY-FF-N$_{ring-centre}$ (Fig. 3**c**). Comparing the interaction energy values in Table 1, both face-to-face configurations displayed similar energies of −12.18 kcal/mol and −12.20 kcal/mol, respectively. Furthermore, the pyrrole nitrogen was also placed on the graphene atom for the GR-PY-FF-N-OnC configuration (**Figure S2g**) and showed a low interaction energy (-11.34 kcal/mol) than former face-to-face cases. The perpendicular configurations shown in **Figure S2e** and **Figure S2h**, interacted through hydrogen atoms from two carbons (GR-PY-Per-2C$_{down}$-On$_{bridge}$) and hydrogen atoms from nitrogen and carbon (GR-PY-Per-N-C$_{down}$-On$_{bridge}$), with bridge of the graphene, exhibited −5.61 and −6.71 kcal/mol, respectively. This is clearly indicated that electronegative nitrogen atom in the pyrrole ring plays an important role for the stronger interaction than carbon atom. The least interaction energy (-4.62 kcal/mol) was obtained for GR-PY-Per-C$_{down-centre}$ (Fig. 3**d**) where hydrogen from one carbon bound to graphene hexagonal ring. Comparing all different configurations of graphene-pyrrole, the adsorbate pyrrole binder molecule appears to form stable configurations face-to-face with graphene rather than sideways orientation; accompanying energy difference is about 5 kcal/mol. This is due to the fact of strong π-π that significantly dominates the π-H interaction.

The graphene-styrene butadiene interaction was comprehensively studied for the configurations (a) graphene-styrene butadiene-perpendicular-phenyl-aliphatic-side-down (GR-SB-Per-PhAl$_{side-down}$), (b)

graphene-styrene butadiene-perpendicular-aliphatic-face (GR-SB-Per-Al-F), (c) graphene- styrene butadiene-perpendicular-phenyl-face (GR-SB-Per-Ph-F), (d) graphene-styrene butadiene-perpendicular-aliphatic-chain-down (GR-SB-Per-Al-C$_{down}$), and (e) graphene-styrene butadiene-perpendicular-phenyl-aliphatic-chain-down (GR-SB-Per-PhAl$_{chain\_down}$). Fig. 4 depicts the configuration of graphene-styrene butadiene from (a) to (d); (e) configuration is shown in **Figure S3**, and the interaction energy of these configurations (a)-(e) is presented in Table 1. In the case of the GR-SB-Per-PhAl$_{side-down}$ configuration, the phenyl ring and alkyl chain in the styrene molecule were perpendicular to the graphene. The interaction of this configuration (a) was found to be −15.79 kcal/mol with an equilibrium distance of 2.837 Å. The butadiene chain was aligned to the graphene-like face-to-face for GR-SB-Per-Al-F (Fig. 4**b**) configuration in which it exhibits −13.29 kcal/mol of interaction energy. However, the highest interaction energy (-15.92 kcal/mol) was obtained for Fig. 4**c** among the investigated graphene-styrene butadiene configurations where the aromatic phenyl ring was faced to the hexagonal ring. While in the case of aliphatic side interaction with graphene, the least interaction energy was obtained, which was about −6.17 kcal/mol. Among the five examined configurations, the highest energy configurations, (a) and (c), are interacting through π-π electron cloud from graphene-aromatic interaction, which is a bit stronger than π-π electron from graphene-alkene interaction (configuration Fig. 4**b**).

We examined several configurations for graphene-acrylonitrile to take into account all possible orientations to evaluate their energies in finding the most viable interactions. In this case, there are nine configurations created: (a) graphene-acrylonitrile-perpendicular-nitrogen-
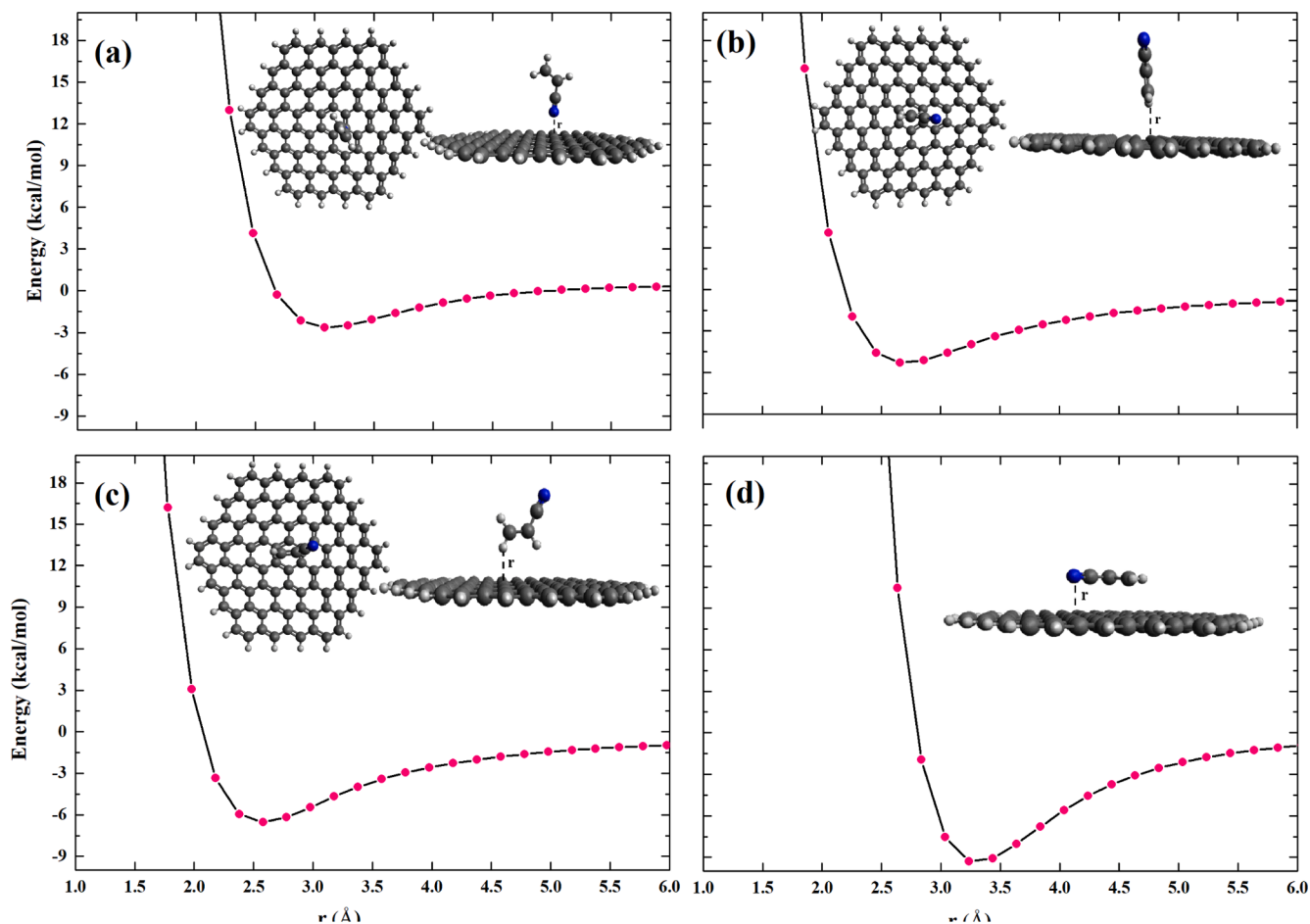
Fig. 5. Interaction energy curves with corresponding structural configuration of graphene-acrylonitrile systems: (a) graphene-acrylonitrile-perpendicular-nitrogen-down-onC (GR-ACN-Per-N$_{down}$-C), (b) graphene-acrylonitrile-perpendicular-methylene-down (GR-ACN-Per-M$_{down}$), (c) graphene-acrylonitrile-perpendicular-acryl-down (GR-ACN-Per-A$_{down}$), and (d) graphene-acrylonitrile-face-face-nitrogen-on-C (GR-ACN-FF-N-onC).

down-onC (GR-ACN-Per-N$_{down}$-C), (b) graphene-acrylonitrile-perpendicular-methylene-down (GR-ACN-Per-M$_{down}$), (c) graphene-acrylonitrile-perpendicular-acryl-down (GR-ACN-Per-A$_{down}$), (d) graphene-acrylonitrile-face-face-nitrogen-on-C (GR-ACN-FF-N-onC), (e) graphene-acrylonitrile-perpendicular-nitrogen-down-center (GR-ACN-Per-N$_{down}$-Cen), (f) graphene-acrylonitrile-perpendicular-nitrogen-down-betweenC (GR-ACN-Per-N$_{down}$-BetC), (g) graphene-acrylonitrile-perpendicular-nitrogen-side-down (GR-ACN-Per-N$_{side\_down}$), (h) graphene-acrylonitrile-face-face-nitrogen-betweenC (GR-ACN-FF-N-BetC), and (i) graphene-acrylonitrile-face-face-nitrogen-center (GR-ACN-FF-N-Cen). In particular, the configurations (a)–(d) are illustrated in Fig. 5, and energy values are collected in Table 1; configurations (e)–(i) with interaction energies are shown in **Figure S4** and **Table S4**. Based on the orientations examined for these configurations, it can be categorized into three types, nitrogen atoms directly interact to graphene ((a), (e), and (f)), face (planar)-graphene interactions ((d), (h), and (i)), and carbon side-graphene interactions ((b), (c), and (g)). The interaction energy of these configurations follows the trend of −9.28 kcal/mol (d) > -9.09 kcal/mol (i) > -8.87 kcal/mol (h) > -6.55 kcal/mol (c) ≈ −6.38 kcal/mol (g) > -5.31 kcal/mol (b) > -3.10 kcal/mol (e) > −2.70 kcal/mol (f) ≈ −2.65 kcal/mol (a). The highest interaction energy was obtained for the GR-ACN-FF-N-onC case, whereas the configuration GR-ACN-Per-N$_{down}$-C exhibited the least energy. This can be due to strong π-electrons interaction from ACN molecule, which happen through face-face interaction to the graphene that significantly dominates the electronegative nitrogen and graphene interaction.

Tetrafluoroethylene (TFE) binder molecule is a planar and consists of

four fluorine atoms attached to the ethylene carbon, and different configurations were studied and shown in Fig. 6 and **Figure S5**. The configuration GR-TFE-Per-1C2F$_{down}$- On$_{Bridge}$ (Fig. 6a) is formed by two fluorine atoms from the same carbon that perpendicularly interacted between carbon atoms in the graphene ring. The interaction energy associated with this particular configuration exhibited the least value of −4.30 kcal/mol with a typical distance of 2.917 Å between C-F. Similarly, in the case of the GR-TFE-Per-1C2F$_{down}$-OnC (**Figure S5e**) configuration, TFE molecule was placed on the carbon atoms, which obtained almost the same interaction energy value as GR-TFE-Per-1C2F$_{down}$-BetC of about −4.74 kcal/mol. It is interesting to note that GR-TFE-Per-2C2F$_{down}$-On$_{Bridge}$ (Fig. 6**b**) and GR-TFE-Per-2C2F$_{down}$-OnC (**Figure S5f**) configurations show the interaction energy values of −4.80 kcal/mol and −4.77 kcal/mol, respectively, which appeared as no significant difference in energy value to those previous configurations (GR-TFE-Per-1C2F$_{down}$-On$_{Bridge}$ and GR-TFE-Per-1C2F$_{down}$-On$_{Bridge}$). These quantified energy values displayed that the interaction of fluorine atoms through perpendicular orientation followed the same interaction irrespective of ethylene carbons. On the other hand, the strongest interaction was obtained for the configuration GR-TFE-FF-On$_{Bridge}$ (Fig. 6**c**) where four fluorine atoms make face-to-face interaction with graphene carbon atoms. The corresponding interaction energy value is −10.07 kcal/mol with a distance of 3.166 Å. However, the interaction energy reduces to −9.33 kcal/mol for the configuration (Fig. 6**d** - GR-TFE-FF-Bet-Ring$_{centre}$) when ethylene bond is placed on the bridge of the graphene carbon atoms. Overall, the face-to-face configurations are significantly higher interaction energy than any of the
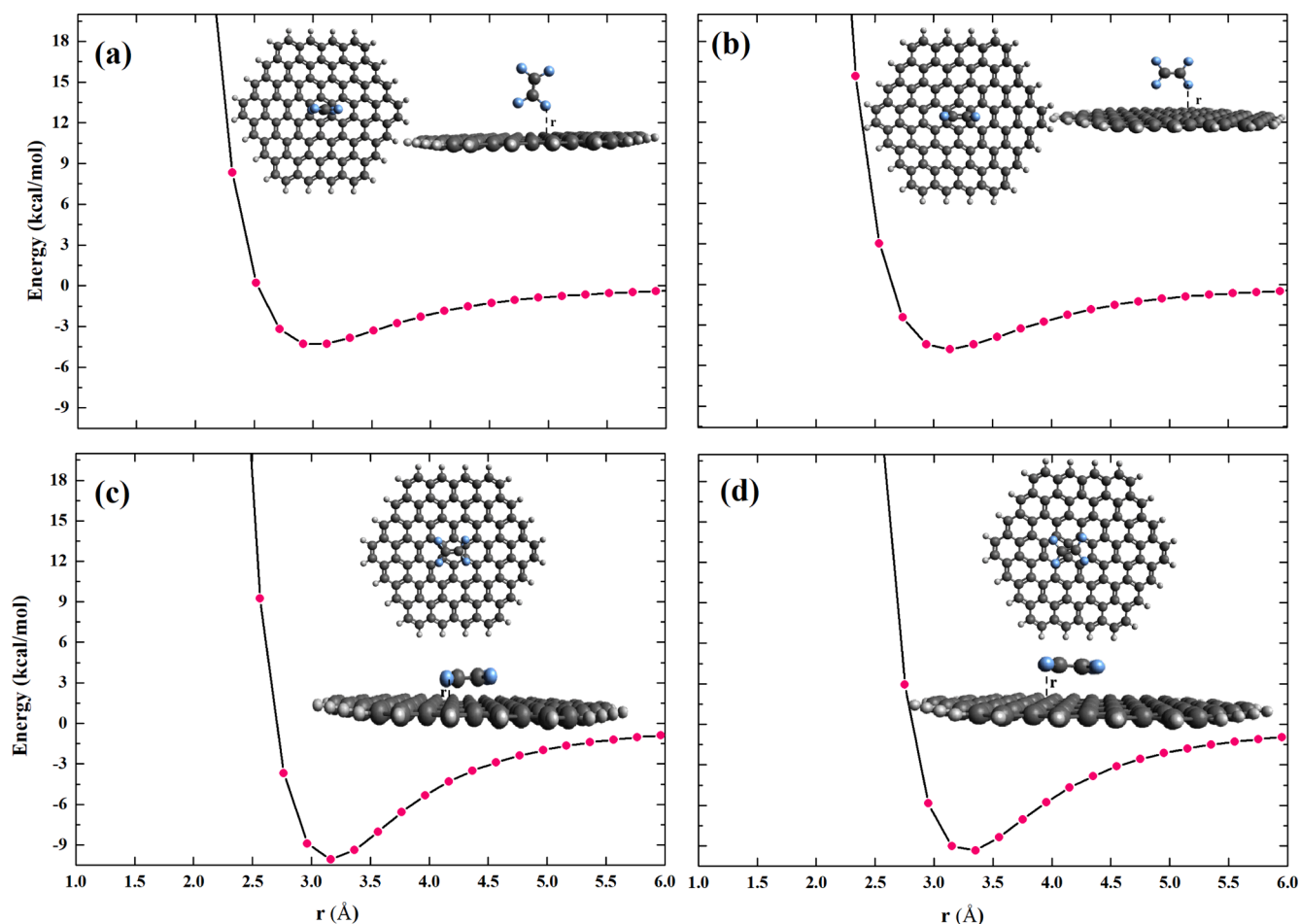
Fig. 6. Interaction energy curves with corresponding structural configuration of graphene- Tetrafluoroethylene (TFE) systems: (a) graphene-tetrafluoroethylene-perpendicular-1carbon-2fluorine-down-on-bridge (GR-TFE-Per-1C2F$_{down}$-On$_{Bridge}$), (b) graphene-tetrafluoroethylene-perpendicular-2carbon-2fluorine-down-on-bridge (GR-TFE-Per-2C2F$_{down}$- On$_{Bridge}$), (c) graphene- tetrafluoroethylene-face-face-on-bridge (GR-TFE-FF-On$_{Bridge}$), and (d) graphene- tetrafluoroethylene-face-face-between-hexagonal-centre (GR-TFE-FF-Bet-Ring$_{centre}$).

perpendicular configurations and the difference of the interaction energy is about 3.5 kcal/mol which is clearly indicated that π electrons made stronger interaction. Moreover, it is interesting to see that comparing TFE with VDF interaction energies in Table 1, explaining the addition of fluorine atoms also greatly impacts the interaction compared to the hydrogen atoms attached to the ethylene carbon atoms. The relative difference of the interaction energy of the most possible configuration these binders such as GR-TFE-FF- On$_{Bridge}$ and GR-VDF-FF-On$_{Bridge}$ is about 2.55 kcal/mol.

Carboxymethyl cellulose (CMC) is one of the sustainable binders used for electrodes fabrication in energy devices, and the possible interaction of CMC with graphene was investigated. Four different configurations are depicted in Fig. 7, and the associated interaction energy values presented in Table 2 and the remaining configurations can be found in **Figure S6** with energy values in **Table S6**. In the case of GR-CMC-Per-RO$_{up}$ (Fig. 7a), the pyranose ring interacted perpendicularly (ring oxygen was facing up) and face-to-face interaction between carboxyl side chain and graphene. The CMC molecule was totally inverted to create a sideways interaction of ring oxygen and carboxylic group, forming GR-CMC-Per-RO$_{down}$ configuration (**Figure S6e**). Both of these configurations exhibit almost similar interaction energy values (-13.55 kcal/mol for GR-CMC-Per-RO$_{up}$ and −13.39 kcal/mol for GR-CMC-Per-RO$_{down}$), showing that the pyranose ring oxygen does not impact the interaction with graphene. However, other examined configurations such as GR-CMC-FF-C-O$_{down}$ (Fig. 7b) and GR-CMC-FF-C-O$_{up}$ (Fig. 7c) are prepared as face-to-face interaction between pyranose ring

and graphene sheet with a difference of carboxyl side chain either facing upward (against graphene) or downward (towards graphene). Comparing these interactions, the GR-CMC-FF-C-O$_{down}$ configuration showed a bit higher interaction energy (-20.33 kcal/mol - highest among all investigated configurations) than GR-CMC-FF-C-O$_{up}$ (-19.59 kcal/mol). The side way interaction of CMC pyranose ring with graphene shown in **Figure S6f** exhibited lower interaction energy, about −9.18 kcal/mol, whereas, the least interaction energy (-6.75 kcal/mol) was obtained for GR-CMC-Per-CO$_{down}$ configuration (Fig. 7d), in which the side carboxylic acid chain was interacted directly to the graphene substrate. The obtained results demonstrated that face-to-face configurations are the dominant configurations compared to perpendicular (or sideways) ones, and the carboxyl side chain enhances the interaction when facing the graphene.

Coumaryl alcohol is one building block of three for lignin polymer that contains aromatic hydroxyl group and aliphatic hydroxyl group attached to the propane side chain. In this case, eight different configurations have been prepared to calculate the interaction energies. Four configurations, (a)–(d), were depicted in Fig. 8 and other configurations can be found in the supporting information (**Figure S7**). The configuration GR-LCmA-Per-Al$_{HO-down}$-Cen in Fig. 8a was constructed by placing aliphatic hydroxyl group at the center of the hexagonal graphene ring to evaluate the interaction, and we found about −5.65 kcal/mol of interaction energy with a distance of 2.562 Å. However, the aromatic hydroxyl group on the graphene carbon atom (GR-LCmA-Per-Ar$_{OH-down}$-OnC) shows the least interaction energy at −5.23 kcal/mol. A
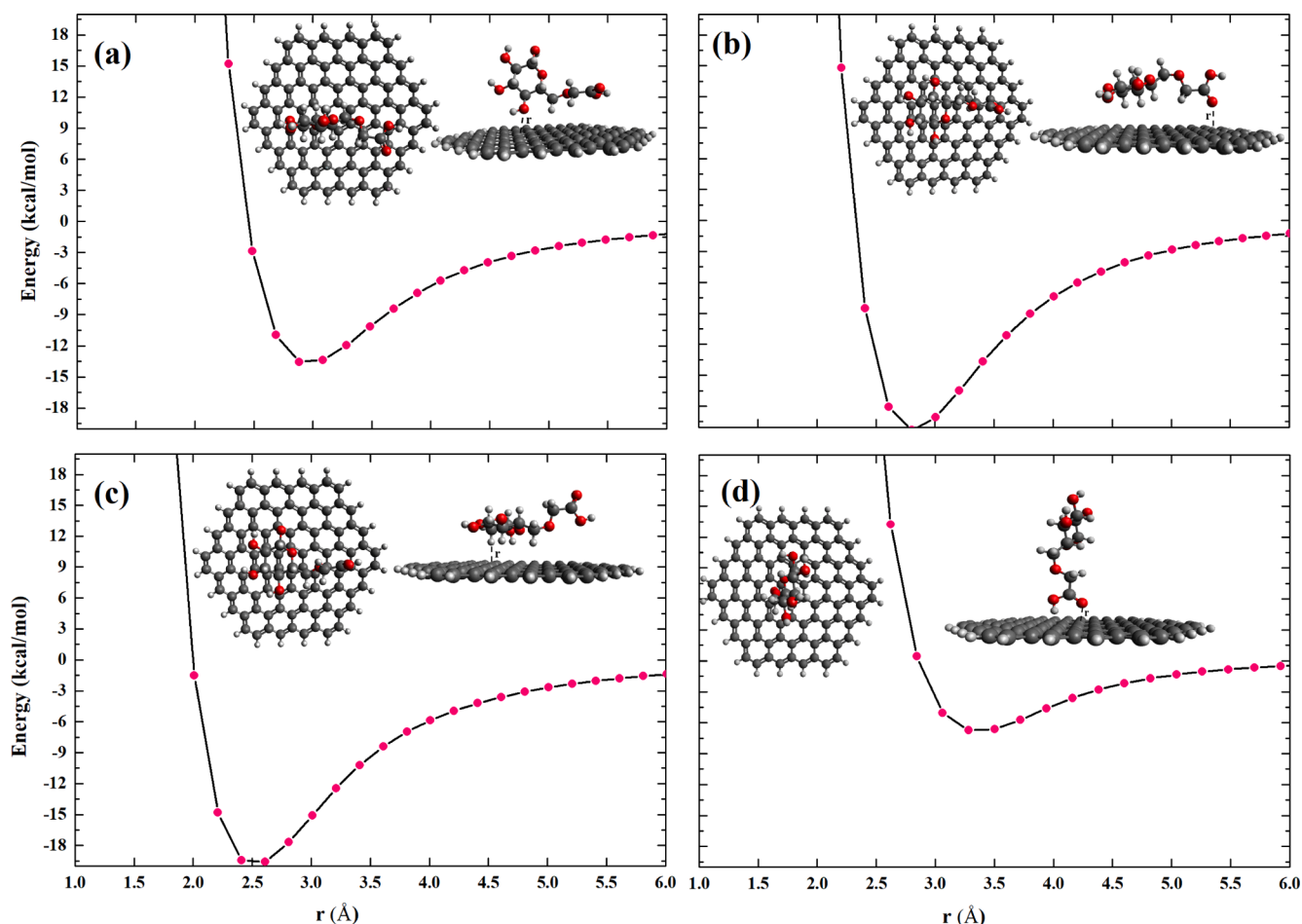
Fig. 7. Interaction energy curves with corresponding structural configuration of graphene- carboxymethylcellulose (CMC) systems: (a) graphene-carboxymethylcellulose-perpendicular-ring-oxygen-up (GR-CMC-Per-RO$_{up}$), (b) graphene-carboxymethylcellulose-face-face-carboxyl-oxygen-down (GR-CMC-FF-C-O$_{down}$), (c) graphene-carboxymethylcellulose-face-face-carboxyl-oxygen-up (GR-CMC-FF-C-O$_{up}$), and (d) graphene-carboxymethylcellulose-perpendicular-carboxyl-group-down (GR-CMC-Per-CO$_{down}$).

Table 2
Name of the configurations, interaction energies (in kcal/mol), and distances between graphene and binders (CMC, LCmA, LCnA, and LSiA) (in Å).

Configurations	Interaction Energy (kcal/mol)	Distance (Å)
Graphene-CMC		
GR-CMC-Per-RO$_{up}$	−13.55	2.886
GR-CMC-FF-C-O$_{down}$	−20.33	2.806
GR-CMC-FF-C-O$_{up}$	−19.59	2.610
GR-CMC-Per-CO$_{down}$	−6.75	3.282
Graphene-LCmA		
GR-LCmA-Per-Al$_{down-center}$	−5.65	2.562
GR-LCmA-Per-Ar$_{down}$-OnC	−5.23	2.896
GR-LCmA-FF-Al-O$_{down}$	−24.00	3.446
GR-LCmA-Per-Side1	−12.51	3.269
Graphene-LCnA		
GR-LCnA-Per-Side	−12.68	2.543
GR-LCnA-FF-Al$_{OH-down}$	−21.10	1.953
GR-LCnA-FF-Al$_{OH-up}$	−26.86	3.069
GR-LCnA-Per-Al$_{OH-down}$	−5.79	3.030
Graphene-LSiA		
GR-LSiA-FF-Al$_{OH-down}$	−25.00	2.009
GR-LSiA-FF-Al$_{OH-up}$	−30.69	3.518
GR-LSiA-Per-Ar$_{OH-down-centre}$	−8.35	2.705
GR-LSiA-Per-Al$_{OH-down}$	−6.57	2.865

similar interaction energy values trend was also observed for the configurations formed with aromatic hydroxyl group interaction (illustrated in **Figure S7e and S7f**), owing to −5.26 kcal/mol and −5.56 kcal/mol

for GR-LCmA-Per-Ar$_{HO-down}$-BetC and GR-LCmA-Per-Ar$_{OH-down}$-OnCen, respectively. It is observed that no significant difference in energy values can be seen for different configurations, formed with perpendicular aromatic-OH or aliphatic side chain-OH with the graphene.

On the other hand, face-to-face interaction shown in Fig. 8c (GR-LCmA-FF-Al$_{HO-down}$) is responsible for the strongest interaction found among the examined graphene-LCmA cases, and the resulting interaction energy is −24.0 kcal/mol, which is due to the fact of favouring strong π-π interaction between phenyl ring and graphene hexagonal rings. The impact of aliphatic hydroxyl group orientation was also tested by facing it against graphene rings (GR-LCmA-FF-Al$_{HO-up}$ - **Figure S7g**), and the obtained results revealed that the interaction energy was found to be lower than that of facing to graphene ring. This finding clearly indicated that the hydroxyl group enhances the interaction with graphene. Other configurations, such as GR-LCmA-Per-Side1 (Fig. 8d) and GR-LCmA-Per-Side2 (**Figure S7h**), show the side way interactions and the values were higher than perpendicular configuration, however, lower than face-to-face configurations.

Like coumaryl alcohol, coniferyl alcohol (guaiacyl unit) also contains the same aromatic moiety but an extra methoxy group is attached in the phenyl ring. The graphene-coniferyl alcohol configurations with different orientations were constructed and presented in Fig. 9 and **Figure S8**. In the case of the GR-LCnA-Per-Side (Fig. 9a) configuration, part of hydrogen atoms from aromatic ring and side chain are interacted with graphene surface and results the interaction energy of −12.68 kcal/mol at 2.543 Å. Similarly, we have also considered other side way
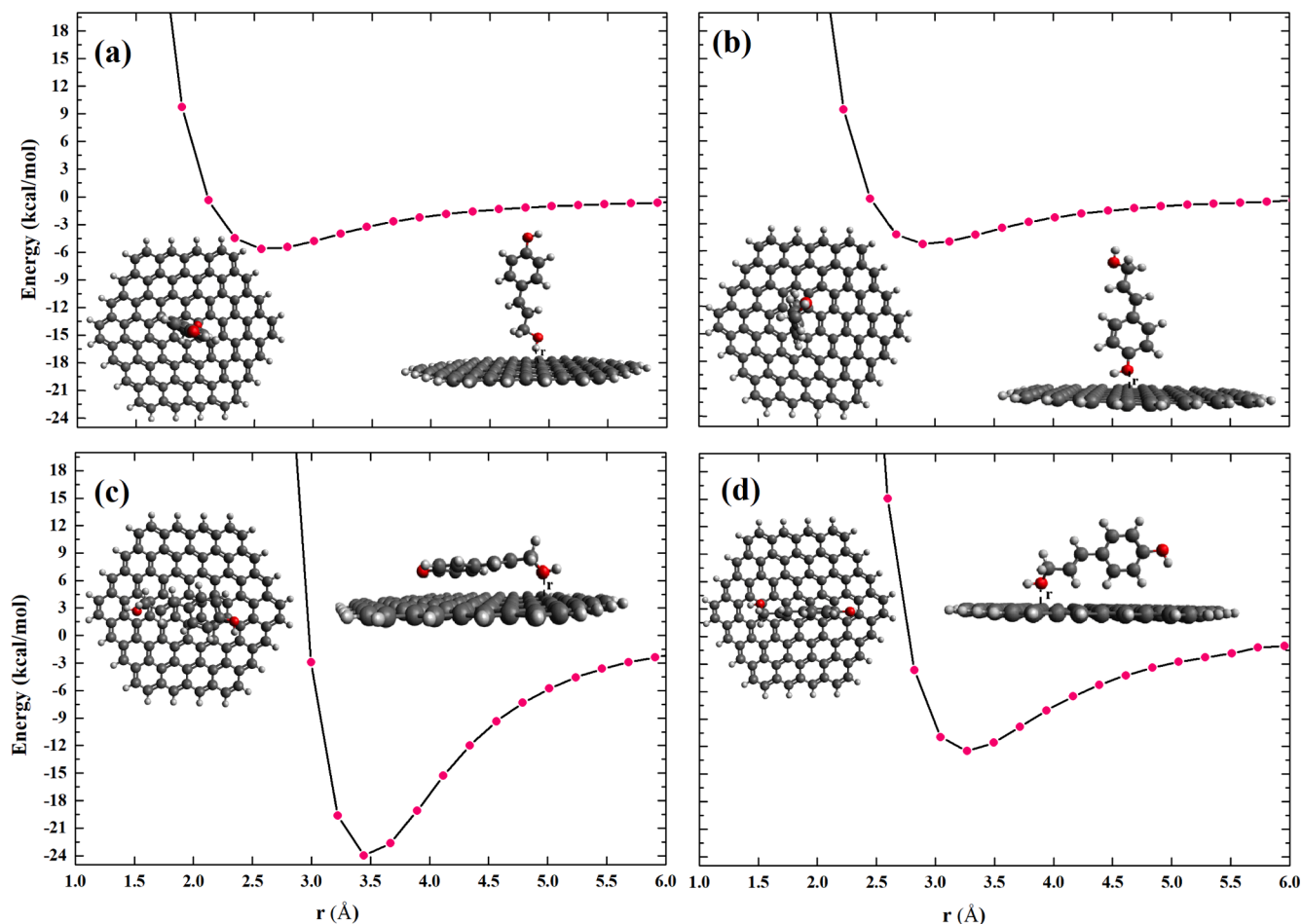
Fig. 8. Interaction energy curves with corresponding structural configuration of graphene- lignin coumaryl alcohol (LCmA) systems: (a) graphene-lignin coumaryl alcohol-perpendicular-aliphatic-OH-down-center (GR-LCmA-Per-Al$_{HO-down}$-Cen), (b) graphene-lignin coumaryl alcohol-perpendicular-aromatic-OH-down-OnC (GR-LCmA-Per-Ar$_{OH-down}$-OnC), (c) graphene-lignin coumaryl alcohol -face-face-aliphatic-OH-down (GR-LCmA-FF-Al$_{HO-down}$), and (d) graphene-lignin coumaryl alcohol-perpendicular -side-1 (GR-LCmA-Per-Side1).

interaction configurations which are perpendicular to the graphene such as LCnA-Per-Ar$_{Methoxy-OH-down}$ (**Figure S8e**), GR-LCnA-Per-Ar$_{OH-side-down}$-On$_{Bridge}$ (**Figure S8f**), GR-LCnA-Per-Ar$_{OH-side-down}$-Cen (**Figure S8g**). In these configurations, either both aromatic hydroxyl and methoxy are close to the graphene (**Figure S8e**) or aromatic hydroxyl and aromatic hydrogen are close to the graphene (**Figure S8f** and **Figure S8g**). The obtained energy values revealed that methoxy group contributes stronger interaction than hydrogen atom, and the associated interaction energy value was about −8.62 kcal/mol for **Figure S8e** than **Figure S8f** (-6.83 kcal/mol) and **Figure S8h** (-7.56 kcal/mol), respectively. Higher interaction energy values were obtained for face-to-face interaction configurations GR-LCnA-FF-Al$_{OH-down}$ (Fig. 9b) and GR-LCnA-FF-Al$_{OH-up}$ (Fig. 9c), of which the latter showed the strongest interaction (-26.86 kcal/mol) rather than the former (-21.10 kcal/mol). The configuration GR-LCnA-Per-Al$_{OH-down}$ shown in Fig. 9d exhibited the least interaction energy among the investigated systems, explaining that aliphatic chain interaction on the graphene make a poor interaction, whereas, the aromatic hydroxyl group interaction from GR-LCnA-Per-Ar$_{OH-down}$-C$_{en}$ configuration (**Figure S8h**) shows a bit of strong interaction energy, about −6.40 kcal/mol. This is clearly indicated that π-electron conjugation significantly impacts for the interaction. It should be emphasized that the addition of methoxy group in the phenyl ring enhances the interaction energy about −3.0 kcal/mol compared to graphene-LCmA systems. Furthermore, aliphatic hydroxyl group hinders the strong π-π electrons interactions in the case of GR-LCnA-FF-Al$_{OH-down}$, whereas no such hindrance is present in the GR-LCnA-FF-

Al$_{OH-up}$ configuration in which the methoxy group in the phenyl ring dominates the aliphatic hydroxy group.

In the case of sinapyl alcohol or syringyl unit, lignin macromolecule contains two methoxy group attached in the phenyl ring and the different types of interactions can be found in Fig. 10. Among these presented configurations of graphene-sinapyl alcohol configurations, like other binders with an aromatic ring, they also exhibited that the face-to-face configurations are the most possible interactions due to the fact of favoring π-π interactions. It is noted that the extra methoxy group in this lignin model shows a great significance in the interaction energies compared to the previous lignin models such as LCmA and LCnA. This is clearly indicated that the extra methoxy group stabilizes the interactions. Comparing these two configurations (GR-LSiA-FF-Al$_{OH-down}$ and GR-LSiA-FF-Al$_{OH-up}$) in Fig. 10**a and 10b**, the aliphatic hydroxyl group against the graphene sheet shows higher interaction energy (-30.69 kcal/mol) because of the free movement of π electrons. We have also considered various possible configuration to evaluate their interaction with graphene, of which the perpendicular arrangement of aliphatic chain interacted with graphene (Fig. 10**d**: GR-LSiA-Per-Al$_{OH-down}$) presents the least interaction energy (-6.57 kcal/mol). Whereas, the configurations shown in Fig. 10**c** (GR-LSiA-Per-Ar$_{OH-down-centre}$), **Figure S9e** (GR-LSiA-Per-Ar$_{OH-down}$-On$_{Bridge}$) and **Figure S9f** (GR-LSiA-Per-Ar$_{OH}$-On-C) exhibit higher interaction energy than the former case. The corresponding obtained energies (-8.34 kcal/mol, −7.67 kcal/mol and −7.86 kcal/mol) implied that no significant difference was observed when distinct configurations were concerned.
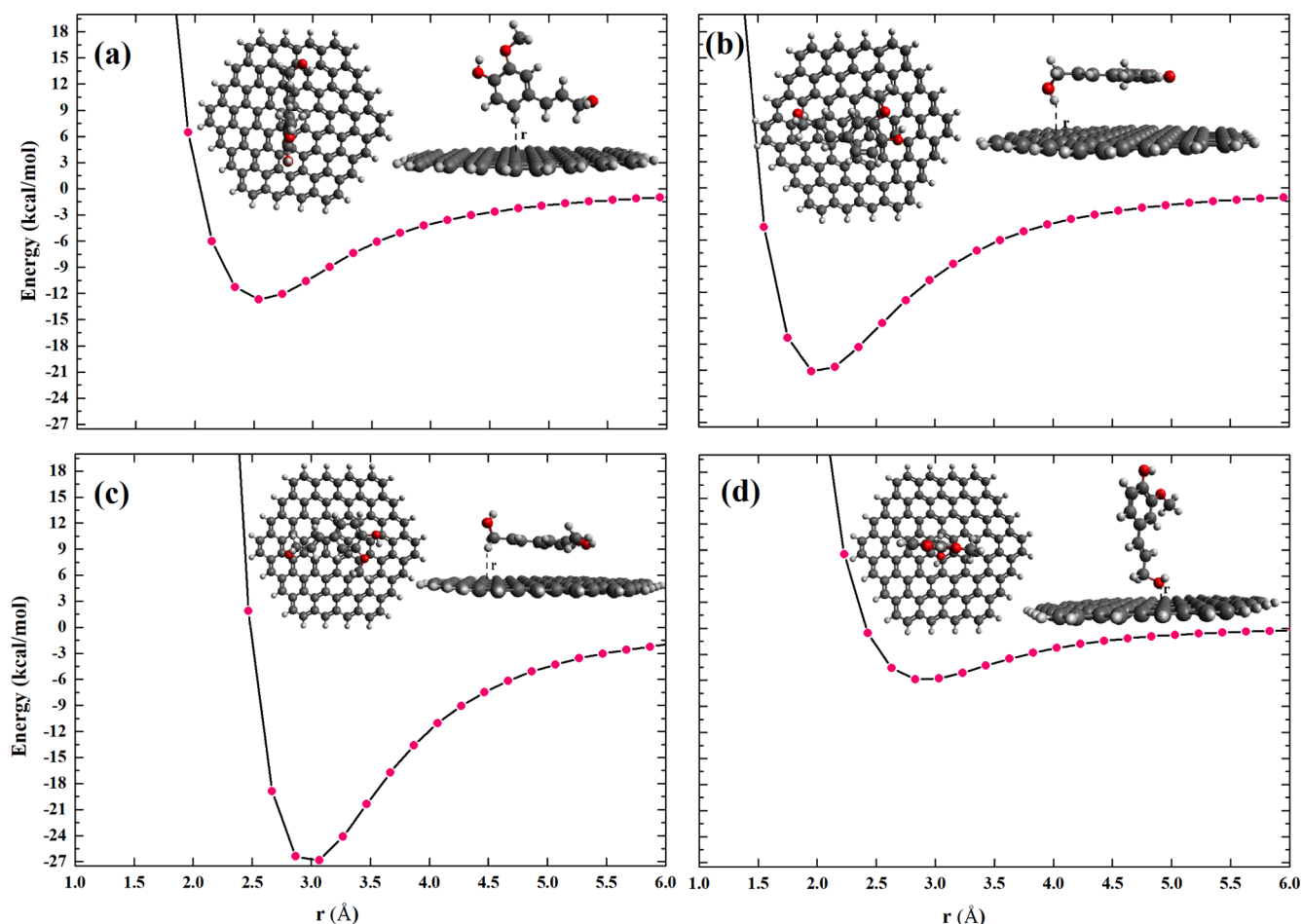
Fig. 9. Interaction energy curves with corresponding structural configuration of graphene- lignin coniferyl alcohol (LCnA) systems: (a) graphene-lignin coniferyl alcohol-perpendicular-aromatic-sideway (GR-LCnA-Per-Side), (b) graphene-lignin coniferyl alcohol-face-face-aliphatic-hydroxyl-down (GR-LCnA-FF-Al$_{OH-down}$), (c) graphene-lignin coniferyl alcohol-face-face-aliphatic-hydroxyl-up (GR-LCnA-FF-Al$_{OH-up}$), and (d) graphene-lignin coniferyl alcohol-perpendicular-aliphatic-hydroxyl-down (GR-LCnA-Per-Al$_{OH-down}$).

4. Discussion

The investigated binders can be grouped based on the raw materials used to produce them like unsustainable (fossil-based) polymers and sustainable polymer materials (biomass-based). The unsustainable binders include VDF, PY, SB, AN, and TFE; CMC, LCmA, LCnA, and LSiA are the sustainable polymers. The most stable interaction values of each binder have been compared in Fig. 11. The order of interaction energy values of graphene with binders is predicted as follows: −30.69 > -26.86 > -24.00 > -20.33 > -15.92 > -12.20 > -10.07 > -9.28 > -7.52 (kcal/mol) for LSiA > LCnA > LCmA > CMC > SB > PY > TFE > ACN > VDF, respectively. It is speculated that sustainable polymers greatly overruled unsustainable polymers, which is very important in order to develop sustainable-based energy materials for energy devices. We also observed that the aromatic ring play an important role, and is responsible for higher interaction energy, which is due to favoring of strong π-π interactions. It can be seen that the molecule with more oxygen atom is strongly adsorbed on the graphene surface for the case of lignin-based binders such as LSiA, LCnA and LCmA because of O-π interactions. This similar trend was observed for the interaction of graphene with other organic molecules [39]. Although, it can be seen strong π-π interaction leads to higher interaction energy and it is interesting to see that CMC molecule attributes strong interaction energy than SB which can be due to large number polar hydroxyl groups predominantly prevail the π-π interaction. It should be emphasized from all configurations, face-to-face arrangement are the most viable structural interactions and

arrangements, which is in good agreement with what the authors reported for benzene and its derivatives[41].

A recent study has attempted to utilize lignin as binders for fabricating both positive and negative electrodes for lithium-ion batteries and the results revealed that the developed electrodes show an excellent capacity with about 148 mAh·g^{-1} and 305 mAh·g^{-1} for the positive and negative electrodes, respectively. However, smaller lignin fractions should be removed prior to the fabrication process. Also, the obtained positive electrodes were thin and therefore require additional processes like modification of lignin to produce thicker electrodes toward enhancing mechanical properties[20]. In the case CMC binder, a recent review implies that CMC is capable of substituting synthetic PVDF binder at the industrial scale due to its higher strong strength between CMC and current collector [54]. Similar comparison study was performed for CMC and PVDF with anatase TiO$_2$ in 2012 and demonstrated that CMC provides good adhesion between active material and current collector and the main advantage is that Na-CMC can be proceed in water[1]. Furthermore, the combination of CMC-SB showed a similar performance as conventional PVDF[16].

The size of the graphene sheet was studied by decreasing as well as increasing the number of carbon atoms (hexagonal rings) to evaluate the impact of interaction energy associated with the size effect. In this regard, the most stable lignin configuration, shown in Fig. 10**b** was chosen and the obtained results were plotted for different examined carbon atoms such as C54 (C$_{54}$H$_{18}$), C96 (C$_{96}$H$_{24}$), and C150 (C$_{150}$H$_{30}$) and shown in Fig. 12. The interaction energy and the distance between
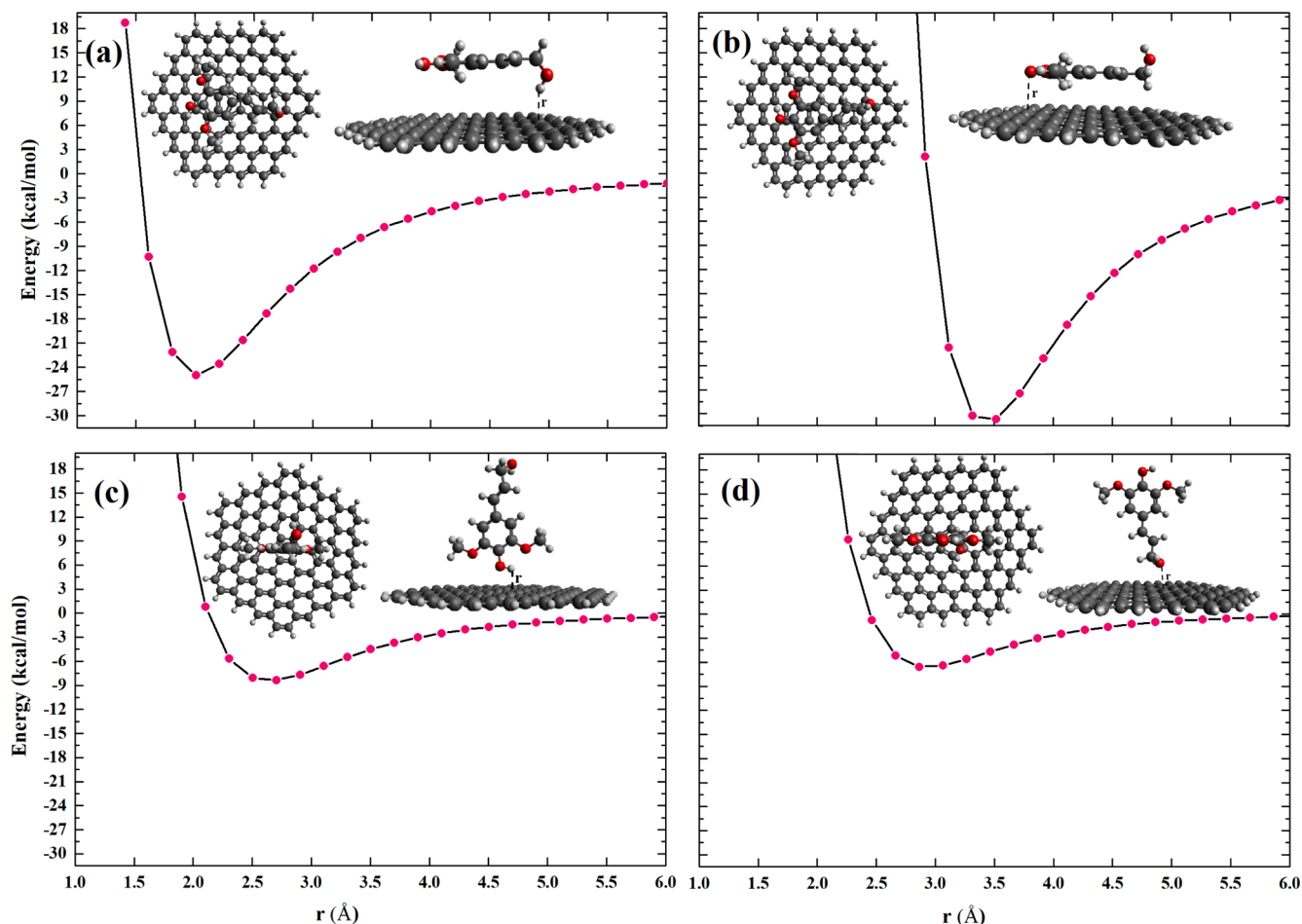
Fig. 10. Interaction energy curves with corresponding structural configuration of graphene- lignin sinapylalcohol (LSiA) systems: (a) graphene-lignin sinapyl alcohol- face-face-aliphatic-hydroxyl-down (GR-LSiA-FF-Al$_{OH-down}$), (b) graphene-lignin sinapyl alcohol- face-face-aliphatic-hydroxyl-up (GR-LSiA-FF-Al$_{OH-up}$), (c) graphene-lignin sinapyl alcohol- perpendicular-aromatic-hydroxyl-down-centre (GR-LSiA-Per-Ar$_{OH-down-centre}$), and (d) graphene-lignin sinapyl alcohol-perpendicular-aliphatic-hydroxyl-down (GR-LSiA-Per-Al$_{OH-down}$).
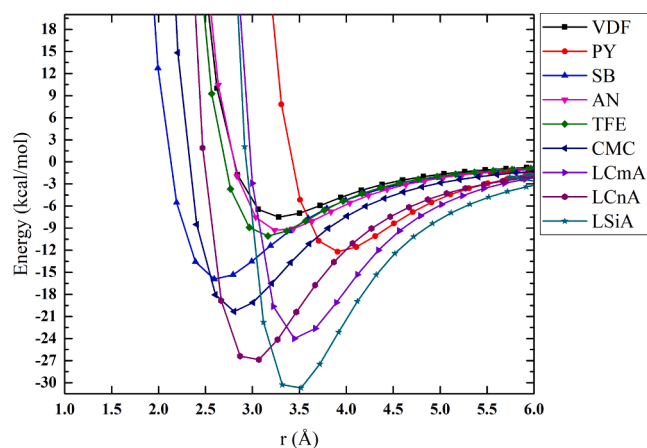
Fig. 11. Comparison of the most possible graphene-binders interaction energy values.

graphene-C and aromatic-O are presented in Table 3. It is seen from Table 3 that the relative difference of interaction energy associated between C54 and C96 is about 2 kcal/mol, however, the difference between C96 and C150 is about 0.4 kcal/mol. These differences in energy values related to the distinct size of the graphene sheet were in closer agreement with the reported values in the reference[37] where authors

have performed the interaction between polyaromatic carbons with water. Furthermore, a similar trend was observed for the minimum energy interaction energy region for the investigated systems with the most stable configuration was found in the distance range between 3.518 and 3.583 Å. This is clearly indicated that the obtained interaction energy for C96 and C150 is negligible compared to the one between C54 and C96 and therefore, the graphene sheet formed by 96 carbon atoms (C$_{96}$H$_{24}$) was extensively used in this study to minimize the computational cost.

5. Conclusions

Density functional theory (DFT) calculations have been employed to evaluate the interaction strength of different binders with graphene. There are nine different binders that were evaluated: vinylidene fluoride (VDF), pyrrole (PY), styrene-butadiene (SB), acrylonitrile (AN), tetrafluoroethylene (TFE), carboxymethylcellulose (CMC), and lignin monomers, coumaryl alcohol (LCmA), coniferyl alcohol (LCnA), and sinapyl alcohol (LSiA). The interaction energy of each graphene-binder system was studied by taking into account all possible orientations on the graphene surface. The examined binders can be grouped into unsustainable (VDF, PY, SB, AN, and TFE) and sustainable (CMC, LCmA, LiCnA, and LSiA) binders. The sustainable binders have demonstrated higher interaction energy compared to unsustainable binders with graphene. Among the sustainable binders, lignin monomers (LCmA, LiCnA, and LSiA) showed a stronger interaction with graphene than graphene-
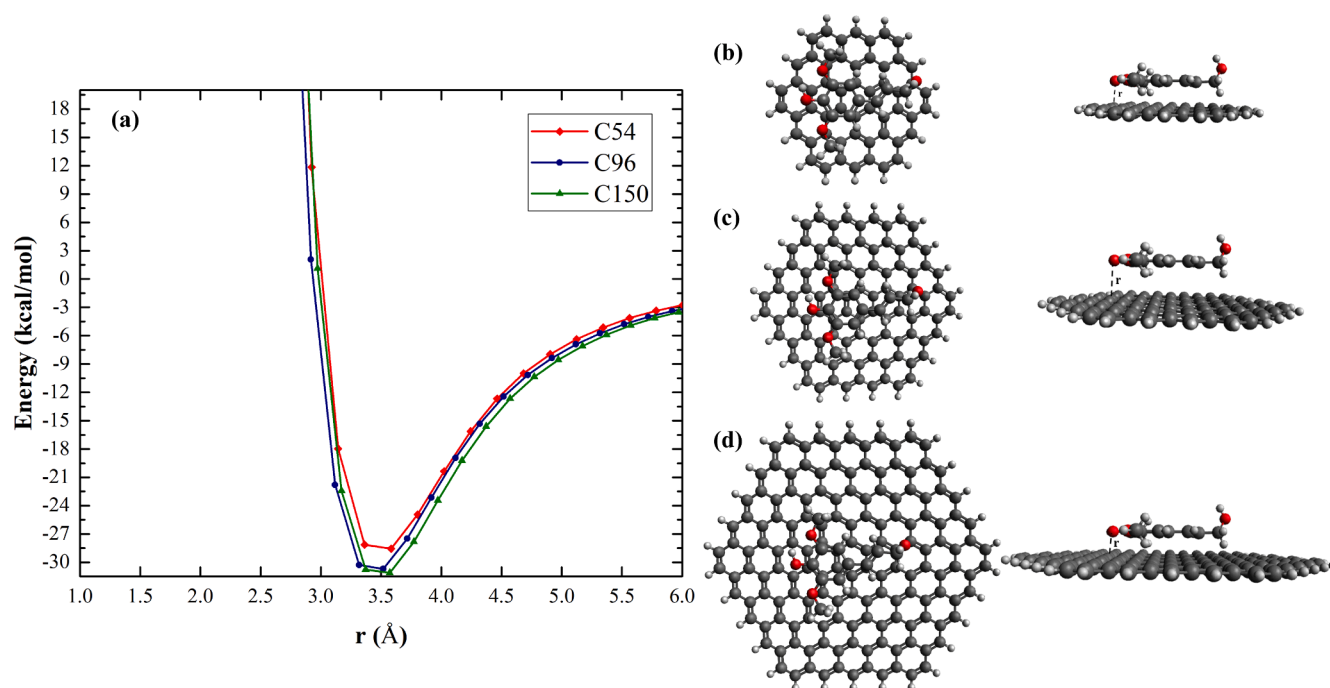
Fig. 12. (a) Comparison of interaction energy curves of graphene-lignin sinapyl alcohol- face-face-aliphatic-hydroxyl-up configuration with respect to the number of carbon atoms in the graphene sheet, (b) C54, (c) C96 and (d) C150.

Table 3
Name of the configurations, interaction energies (in kcal/mol), and distances between different size of the graphene-C and aromatic-O from lignin sinapyl alcohol (in Å).

Configurations	Interaction Energy (kcal/mol)	Distance (Å)
C54-LSiA	−28.56	3.583
C96-LSiA	−30.69	3.518
C150-LSiA	−31.10	3.572

CMC. Overall, the interaction energy of the binder with graphene was : $-30.69 > -26.86 > -24.00 > -20.33 > -15.92 > -12.20 > -10.07 > -9.28 > -7.52$ (kcal/mol) for LSiA > LCnA > LCmA > CMC > SB > PY > TFE > AN > VDF, respectively. The size of the graphene was also considered to evaluate the size effect and the results have shown that the relative difference between the interaction energy of the C54 ($C_{54}H_{18}$) and C96 ($C_{96}H_{24}$) is about 2 kcal/mol, however, the difference between C96 and C150 ($C_{150}H_{30}$) is about 0.4 kcal/mol. This is clearly indicated that the chosen graphene C96 ($C_{96}H_{24}$) is sufficient to study the interaction between graphene and the examined binder molecules.

The most stable or the highest interaction energy was obtained for each binder case when the molecule interacts face-to-face with the graphene surface. This is due to the fact of a higher possibility for π-π interactions, which strongly binds together with graphene hexagonal rings. The substituent group strengthens the interaction between lignin monomers with graphene, of which the higher amount of methoxy group in the aromatic ring, the higher the interaction energies for LSiA binder. In the case of CMC, the carboxyl group in the side chain is responsible for stronger interaction with graphene. On the other hand, among unsustainable-based binders, SB possesses the highest interaction, followed by PY binder. This explains that the aromatic π-electron cloud overrules aliphatic π-electron with graphene. These proposed results boost the valorization of lignocellulosic biomass components in order to develop high value-added sustainable materials and are expected to provide extensive support for designing novel sustainable energy devices.

CRediT authorship contribution statement

Veerapandian Ponnuchamy: Conceptualization, Investigation, Formal analysis, Visualization, Methodology, Visualization, Writing – original draft. **Esakkiammal Sudha Esakkimuthu:** Conceptualization, Investigation, Formal analysis, Visualization, Methodology, Visualization, Writing – original draft.

Declaration of Competing Interest

The authors declare that they have no known competing financial interests or personal relationships that could have appeared to influence the work reported in this paper.

Acknowledgements

Appendix A. Supplementary material

Supplementary data to this article can be found online at https://doi.org/10.1016/j.apsusc.2021.151461.

References

[1] M. Mancini, F. Nobili, R. Tossici, R. Marassi, Study of the electrochemical behavior at low temperatures of green anodes for Lithium ion batteries prepared with anatase TiO2 and water soluble sodium carboxymethyl cellulose binder,

Electrochim. Acta 85 (2012) 566–571, https://doi.org/10.1016/j.electacta.2012.08.115.

[2] M. Manickam, M. Takata, Effect of cathode binder on capacity retention and cycle life in transition metal phosphate of a rechargeable lithium battery, Electrochim. Acta 48 (8) (2003) 957–963, https://doi.org/10.1016/S0013-4686(02)00808-3.

[3] A. Guerfi, M. Kaneko, M. Petitclerc, M. Mori, K. Zaghib, LiFePO4 water-soluble binder electrode for Li-ion batteries, J. Power Sources 163 (2) (2007) 1047–1052, https://doi.org/10.1016/j.jpowsour.2006.09.067.

[4] S.J. Rezvani, M. Pasqualini, A. Witkowska, R. Gunnella, A. Birrozzi, M. Minicucci, H. Rajantie, M. Copley, F. Nobili, A. Di Cicco, Binder-induced surface structure evolution effects on Li-ion battery performance, Appl. Surf. Sci. 435 (2018) 1029–1036, https://doi.org/10.1016/j.apsusc.2017.10.195.

[5] V.H. Nguyen, W.L. Wang, E.M. Jin, H.-B. Gu, Impacts of different polymer binders on electrochemical properties of LiFePO4 cathode, Appl. Surf. Sci. 282 (2013) 444–449, https://doi.org/10.1016/j.apsusc.2013.05.149.

[6] N.-S. Choi, S.-Y. Ha, Y. Lee, J.Y. Jang, M.-H. Jeong, W.C. Shin, M. Ue, Recent Progress on Polymeric Binders for Silicon Anodes in Lithium-Ion Batteries, J. Electrochem. Sci. Technol. 6 (2) (2015) 35–49, https://doi.org/10.5229/JECST.2015.6.2.35.

[7] J.-I. Lee, H. Kang, K.H. Park, M. Shin, D. Hong, H.J. Cho, N.-R. Kang, J. Lee, S. M. Lee, J.-Y. Kim, C.K. Kim, H. Park, N.-S. Choi, S. Park, C. Yang, Amphiphilic Graft Copolymers as a Versatile Binder for Various Electrodes of High-Performance Lithium-Ion Batteries, Small. 12 (23) (2016) 3119–3127, https://doi.org/10.1002/smll.v12.2310.1002/smll.201600800.

[8] S.-J. Park, H. Zhao, G. Ai, C. Wang, X. Song, N. Yuca, V.S. Battaglia, W. Yang, G. Liu, Side-Chain Conducting and Phase-Separated Polymeric Binders for High-Performance Silicon Anodes in Lithium-Ion Batteries, J. Am. Chem. Soc. 137 (7) (2015) 2565–2571, https://doi.org/10.1021/ja511181p.

[9] T.C. Nirmale, B.B. Kale, A.J. Varma, A review on cellulose and lignin based binders and electrodes: Small steps towards a sustainable lithium ion battery, Int. J. Biol. Macromol. 103 (2017) 1032–1043, https://doi.org/10.1016/j.ijbiomac.2017.05.155.

[10] T. Zhang, L. Yang, X. Yan, X. Ding, Recent Advances of Cellulose-Based Materials and Their Promising Application in Sodium-Ion Batteries and Capacitors, Small. 14 (47) (2018) 1802444, https://doi.org/10.1002/smll.v14.4710.1002/smll.201802444.

[11] W. Zaïdi, Y. Oumellal, J.-P. Bonnet, J. Zhang, F. Cuevas, M. Latroche, J.-L. Bobet, L. Aymard, Carboxymethylcellulose and carboxymethylcellulose-formate as binders in MgH2–carbon composites negative electrode for lithium-ion batteries, J. Power Sources 196 (5) (2011) 2854–2857, https://doi.org/10.1016/j.jpowsour.2010.11.048.

[12] The influence of polytetrafluoroethylene reduction on the capacity loss of the carbon anode for lithium ion batteries, Solid State Ionics. 90 (1996) 221–225. https://doi.org/10.1016/S0167-2738(96)00367-0.

[13] S.-L. Chou, X.-W. Gao, J.-Z. Wang, D. Wexler, Z.-X. Wang, L.-Q. Chen, H.-K. Liu, Tin/ polypyrrole composite anode using sodium carboxymethyl cellulose binder for lithium-ion batteries, Dalton Trans. 40 (2011) 12801–12807, https://doi.org/10.1039/C1DT10396B.

[14] Electrochemical and X-ray photospectroscopy studies of polytetrafluoroethylene and polyvinylidene fluoride in Li/C batteries, J. Power Sources. 68 (1997) 344–347. https://doi.org/10.1016/S0378-7753(97)02637-2.

[15] L. Gong, M.H.T. Nguyen, E.-S. Oh, High polar polyacrylonitrile as a potential binder for negative electrodes in lithium ion batteries, Electrochem. Commun. 29 (2013) 45–47, https://doi.org/10.1016/j.elecom.2013.01.010.

[16] H. Buqa, M. Holzapfel, F. Krumeich, C. Veit, P. Novák, Study of styrene butadiene rubber and sodium methyl cellulose as binder for negative electrodes in lithium-ion batteries, J. Power Sources 161 (1) (2006) 617–622, https://doi.org/10.1016/j.jpowsour.2006.03.073.

[17] X. Gao, W. Luo, C. Zhong, D. Wexler, S.-L. Chou, H.-K. Liu, Z. Shi, G. Chen, K. Ozawa, J.-Z. Wang, Novel Germanium/Polypyrrole Composite for High Power Lithium-ion Batteries, Sci. Rep. 4 (2014) 6095, https://doi.org/10.1038/srep06095.

[18] X. Hong, Y. Liu, Y. Li, X. Wang, J. Fu, X. Wang, Application Progress of Polyaniline Polypyrrole and Polythiophene in Lithium-Sulfur Batteries, Polymers. 12 (2020) 331, https://doi.org/10.3390/polym12020331.

[19] Y. Qi, M.H.T. Nguyen, E.-S. Oh, Effect of conductive polypyrrole in poly (acrylonitrile-co-butyl acrylate) water–based binder on the performance of electrochemical double-layer capacitors, J Solid State Electrochem. 25 (3) (2021) 963–972, https://doi.org/10.1007/s10008-020-04864-z.

[20] H. Lu, A. Cornell, F. Alvarado, M. Behm, S. Leijonmarck, J. Li, P. Tomani, G. Lindbergh, Lignin as a Binder Material for Eco-Friendly Li-Ion Batteries, Materials. 9 (2016) 127, https://doi.org/10.3390/ma9030127.

[21] T. Chen, Q. Zhang, J. Pan, J. Xu, Y. Liu, M. Al-Shroofy, Y.-T. Cheng, Low-Temperature Treated Lignin as Both Binder and Conductive Additive for Silicon Nanoparticle Composite Electrodes in Lithium-Ion Batteries, ACS Appl. Mater. Interfaces. 8 (47) (2016) 32341–32348, https://doi.org/10.1021/acsami.6b1150010.1021/acsami.6b11500.s001.

[22] V.K. Thakur, M.K. Thakur, P. Raghavan, M.R. Kessler, Progress in Green Polymer Composites from Lignin for Multifunctional Applications: A Review, ACS Sustain. Chem. Eng. 2 (5) (2014) 1072–1092, https://doi.org/10.1021/sc500087z.

[23] Q. Liu, L. Luo, L. Zheng, Lignins: Biosynthesis and Biological Functions in Plants, Int. J. Mol. Sci. 19 (2018) 335, https://doi.org/10.3390/ijms19020335.

[24] K. Babeł, K. Jurewicz, KOH activated lignin based nanostructured carbon exhibiting high hydrogen electrosorption, Carbon 46 (14) (2008) 1948–1956, https://doi.org/10.1016/j.carbon.2008.08.005.

[25] M.N. Collins, M. Nechifor, F. Tanasă, M. Zănoagă, A. McLoughlin, M.A. Stróżyk, M. Culebras, C.-A. Teacă, Valorization of lignin in polymer and composite systems for advanced engineering applications – A review, Int. J. Biol. Macromol. 131 (2019) 828–849, https://doi.org/10.1016/j.ijbiomac.2019.03.069.

[26] L. Cao, I.K.M. Yu, Y. Liu, X. Ruan, D.C.W. Tsang, A.J. Hunt, Y.S. Ok, H. Song, S. Zhang, Lignin valorization for the production of renewable chemicals: State-of-the-art review and future prospects, Bioresour. Technol. 269 (2018) 465–475, https://doi.org/10.1016/j.biortech.2018.08.065.

[27] J. Hayashi, A. Kazehaya, K. Muroyama, A.P. Watkinson, Preparation of activated carbon from lignin by chemical activation, Carbon 38 (13) (2000) 1873–1878, https://doi.org/10.1016/S0008-6223(00)00027-0.

[28] K. Zhang, M. Liu, T. Zhang, X. Min, Z. Wang, L. Chai, Y. Shi, High-performance supercapacitor energy storage using a carbon material derived from lignin by bacterial activation before carbonization, J. Mater. Chem. A. 7 (47) (2019) 26838–26848, https://doi.org/10.1039/C9TA04369A.

[29] J.H. Park, H.H. Rana, J.Y. Lee, H.S. Park, Renewable flexible supercapacitors based on all-lignin-based hydrogel electrolytes and nanofiber electrodes, J. Mater. Chem. A. 7 (28) (2019) 16962–16968, https://doi.org/10.1039/C9TA03519B.

[30] C. Ma, Z. Li, J. Li, Q. Fan, L. Wu, J. Shi, Y. Song, Lignin-based hierarchical porous carbon nanofiber films with superior performance in supercapacitors, Appl. Surf. Sci. 456 (2018) 568–576, https://doi.org/10.1016/j.apsusc.2018.06.189.

[31] Y. Li, Y.-S. Hu, H. Li, L. Chen, X. Huang, A superior low-cost amorphous carbon anode made from pitch and lignin for sodium-ion batteries, J. Mater. Chem. A. 4 (1) (2016) 96–104, https://doi.org/10.1039/C5TA08601A.

[32] L. Du, W. Wu, C. Luo, H. Zhao, D. Xu, R. Wang, Y. Deng, Lignin derived Si@C composite as a high performance anode material for lithium ion batteries, Solid State Ionics 319 (2018) 77–82, https://doi.org/10.1016/j.ssi.2018.01.039.

[33] C. Luo, L. Du, W. Wu, H. Xu, G. Zhang, S. Li, C. Wang, Z. Lu, Y. Deng, Novel Lignin-Derived Water-Soluble Binder for Micro Silicon Anode in Lithium-Ion Batteries, ACS Sustain. Chem. Eng. 6 (10) (2018) 12621–12629, https://doi.org/10.1021/acssuschemeng.8b01161.

[34] D. Aurbach, H. Teller, M. Koltypin, E. Levi, On the behavior of different types of graphite anodes, J. Power Sources 119–121 (2003) 2–7, https://doi.org/10.1016/S0378-7753(03)00115-0.

[35] F. Cao, I.V. Barsukov, H.J. Bang, P. Zaleski, J. Prakash, Evaluation of Graphite Materials as Anodes for Lithium-Ion Batteries, J. Electrochem. Soc. 147 (10) (2000) 3579, https://doi.org/10.1149/1.1393942.

[36] Q. Cheng, Y. Okamoto, N. Tamura, M. Tsuji, S. Maruyama, Y. Matsuo, Graphene-Like-Graphite as Fast-Chargeable and High-Capacity Anode Materials for Lithium Ion Batteries, Sci Rep. 7 (2017) 14782, https://doi.org/10.1038/s41598-017-14504-8.

[37] A.O. Ajala, V. Voora, N. Mardirossian, F. Furche, F. Paesani, Assessment of Density Functional Theory in Predicting Interaction Energies between Water and Polycyclic Aromatic Hydrocarbons: from Water on Benzene to Water on Graphene, J. Chem. Theory Comput. 15 (4) (2019) 2359–2374, https://doi.org/10.1021/acs.jctc.9b00110.

[38] E.V. Raksha, Y.B. Vysotsky, E.S. Kartashynska, M.V. Savoskin, Formation of carboxylic acid complexes with polyaromatic hydrocarbons of the coronene series. Quantum chemical modelling, J. Phys.: Conf. Ser. 1658 (2020) 012044, https://doi.org/10.1088/1742-6596/1658/1/012044.

[39] J. Yang, J. Yuan, Z. Hua, Density functional theory study of interaction of graphene with hypoxanthine, xanthine, and uric acid, Mol. Phys. 114 (14) (2016) 2157–2163, https://doi.org/10.1080/00268976.2016.1189009.

[40] K. Kato, T. Iyama, H. Tachikawa, Density Functional Theory Study of the Interaction of Magnesium Ions with Graphene Chip, Jpn. J. Appl. Phys. 50 (2011) 01BJ01, https://doi.org/10.1143/JJAP.50.01BJ01.

[41] E.E. de Moraes, M.Z. Tonel, S.B. Fagan, M.C. Barbosa, Density functional theory study of π-aromatic interaction of benzene, phenol, catechol, dopamine isolated dimers and adsorbed on graphene surface, J Mol Model. 25 (2019) 302, https://doi.org/10.1007/s00894-019-4185-2.

[42] S. Güryel, M. Alonso, B. Hajgató, Y. Dauphin, G. Van Lier, P. Geerlings, F. De Proft, A computational study on the role of noncovalent interactions in the stability of polymer/graphene nanocomposites, J Mol Model. 23 (2017) 43, https://doi.org/10.1007/s00894-017-3214-2.

[43] S. Abe, Y. Nagoya, F. Watari, H. Tachikawa, Evaporation processes of water molecules from graphene edge: DFT and MD study, Comput. Mater. Sci. 50 (9) (2011) 2640–2643, https://doi.org/10.1016/j.commatsci.2011.04.009.

[44] M.W. Schmidt, K.K. Baldridge, J.A. Boatz, S.T. Elbert, M.S. Gordon, J.H. Jensen, S. Koseki, N. Matsunaga, K.A. Nguyen, S. Su, T.L. Windus, M. Dupuis, J. A. Montgomery, General atomic and molecular electronic structure system, J. Comput. Chem. 14 (11) (1993) 1347–1363, https://doi.org/10.1002/jcc.540141112.

[45] V. Ponnuchamy, O. Gordobil, R.H. Diaz, A. Sandak, J. Sandak, Fractionation of lignin using organic solvents: A combined experimental and theoretical study, Int. J. Biol. Macromol. 168 (2021) 792–805, https://doi.org/10.1016/j.ijbiomac.2020.11.139.

[46] V. Ponnuchamy, A. Sandak, J. Sandak, Multiscale modelling investigation of wood modification with acetic anhydride, PCCP 22 (48) (2020) 28448–28458, https://doi.org/10.1039/D0CP05165A.

[47] J.-D. Chai, M. Head-Gordon, Long-range corrected hybrid density functionals with damped atom–atom dispersion corrections, Phys. Chem. Chem. Phys. 10 (2008) 6615–6620, https://doi.org/10.1039/B810189B.

[48] J.D. Kubicki, M.-A. Mohamed, H.D. Watts, Quantum mechanical modeling of the structures, energetics and spectral properties of Iα and Iβ cellulose, Cellulose 20 (1) (2013) 9–23, https://doi.org/10.1007/s10570-012-9838-6.

[49] M. Cirtog, M.E. Alikhani, B. Madebène, P. Soulard, P. Asselin, B. Tremblay, Bonding Nature and Vibrational Signatures of Oxirane:(Water)n=1–3. Assessment of the Performance of the Dispersion-Corrected DFT Methods Compared to the ab initio Results and Fourier Transform Infrared Experimental Data, J. Phys. Chem. A. 115 (24) (2011) 6688–6701, https://doi.org/10.1021/jp202867t.

[50] E.G. Gordeev, M.V. Polynski, V.P. Ananikov, Fast and accurate computational modeling of adsorption on graphene: a dispersion interaction challenge, Phys. Chem. Chem. Phys. 15 (2013) 18815–18821, https://doi.org/10.1039/C3CP53189A.

[51] O.V. Ershova, T.C. Lillestolen, E. Bichoutskaia, Study of polycyclic aromatic hydrocarbons adsorbed on graphene using density functional theory with empirical dispersion correction, PCCP 12 (2010) 6483–6491, https://doi.org/10.1039/C000370K.

[52] W. Wang, T. Sun, Y.u. Zhang, Y.-B. Wang, Benchmark calculations of the adsorption of aromatic molecules on graphene, J. Comput. Chem. 36 (23) (2015) 1763–1771, https://doi.org/10.1002/jcc.v36.2310.1002/jcc.23994.

[53] M. Pokora, P. Paneth, Can Adsorption on Graphene be Used for Isotopic Enrichment? A DFT Perspective, Molecules. 23 (2018) 2981, https://doi.org/10.3390/molecules23112981.

[54] S. Li, Y.-M. Liu, Y.-C. Zhang, Y. Song, G.-K. Wang, Y.-X. Liu, Z.-G. Wu, B.-H. Zhong, Y.-J. Zhong, X.-D. Guo, A review of rational design and investigation of binders applied in silicon-based anodes for lithium-ion batteries, J. Power Sources 485 (2021) 229331, https://doi.org/10.1016/j.jpowsour.2020.229331.